

## THE APPLICATION OF MULTIVIEW METHODS FOR HIGH-PRECISION ASTROMETRIC SPACE VLBI AT LOW FREQUENCIES

R. DODSON<sup>1,2</sup>, M. RIOJA<sup>1,3</sup>, Y. ASAKI<sup>4,5</sup>, H. IMAI<sup>1,6</sup>, X.-Y. HONG<sup>7</sup>, AND Z. SHEN<sup>7</sup>

<sup>1</sup> International Centre for Radio Astronomy Research, M468, The University of Western Australia, 35 Stirling Hwy, Crawley, Western Australia 6009, Australia; [richard.dodson@icrar.org](mailto:richard.dodson@icrar.org)

<sup>2</sup> Korea Astronomy and Space Science Institute, Daejeon 305-348, Korea

<sup>3</sup> Observatorio Astronómico Nacional (OAN), Apartado 112, E-28803 Alcala de Henares, Spain

<sup>4</sup> Institute of Space and Astronautical Science, 3-1-1 Yoshinodai, Chuou, Sagami-hara, Kanagawa 252-5210, Japan

<sup>5</sup> Department of Space and Astronautical Science, School of Physical Sciences, The Graduate University of Advanced Studies (SOKENDAI), 3-1-1 Yoshinodai, Chuou, Sagami-hara, Kanagawa 252-5210, Japan

<sup>6</sup> Department of Physics and Astronomy, Graduate School of Science and Engineering, Kagoshima University, 1-21-35 Korimoto, Kagoshima 890-0065, Japan

<sup>7</sup> Shanghai Astronomical Observatory, CAS, 200030 Shanghai, China

Received 2012 December 12; accepted 2013 March 13; published 2013 April 30

### ABSTRACT

High-precision astrometric space very long baseline interferometry (S-VLBI) at the low end of the conventional frequency range, i.e., 20 cm, is a requirement for a number of high-priority science goals. These are headlined by obtaining trigonometric parallax distances to pulsars in pulsar–black hole pairs and OH masers anywhere in the Milky Way and the Magellanic Clouds. We propose a solution for the most difficult technical problems in S-VLBI by the MultiView approach where multiple sources, separated by several degrees on the sky, are observed simultaneously. We simulated a number of challenging S-VLBI configurations, with orbit errors up to 8 m in size and with ionospheric atmospheres consistent with poor conditions. In these simulations we performed MultiView analysis to achieve the required science goals. This approach removes the need for beam switching requiring a Control Moment Gyro, and the space and ground infrastructure required for high-quality orbit reconstruction of a space-based radio telescope. This will dramatically reduce the complexity of S-VLBI missions which implement the phase-referencing technique.

*Key words:* space vehicles: instruments – techniques: high angular resolution – techniques: interferometric

*Online-only material:* color figures

### 1. INTRODUCTION

Astrometry has had limited application in space very long baseline interferometry (S-VLBI; Rioja et al. 2009b; Guirado et al. 2001), as the existing missions (HALCA (Hirabayashi et al. 2000) and RadioAstron (Kardashev 1997)) were designed without the rapid beam-switching capability traditionally required for phase referencing (PR). The VSOP-2 (ASTRO-G) mission was designed with this capability, but has been cancelled due to insufficient technical readiness, mainly in the surface accuracies of the main reflector that was required for the highest frequencies. The ASTRO-G design, however, included the infrastructure for PR, that is: the capability for rapid source switching with attitude control (requiring a massive gyroscope) and accurate orbit determination (requiring the application of multiple complex spacecraft navigation methods). In this paper, we investigate the possibilities of using MultiView VLBI as an alternative method to address the requirements and find that this approach offers a solution for these aspects of PR S-VLBI on future missions.

S-VLBI is recognized as one of the most challenging areas of VLBI, as it—as for all space missions—requires the manufacturing of complex technologies, which must be space certified to survive long exposure to high levels of cosmic radiation, which must be robust enough to survive the launch, which must be reliable enough to operate without maintenance for the full lifetime of the mission—typically three or more years—and yet be light enough to not overwhelm the extremely restricted weight budget of any satellite launch. In addition, there are the

complications arising from the sensitivity of the space-based antenna. This relates to the unfolding of a large parabolic reflector in space while ensuring that the surface accuracy is sufficiently high for observation at the highest frequencies and downlinking a large bandwidth of coherent baseband radio data to the ground tracking stations. Furthermore for conventional PR S-VLBI the instantaneous satellite position needs to be known to a high degree of accuracy. In Asaki et al. (2007) a careful study of the requirements for PR observing at the ASTRO-G frequencies of 8, 22, and 43 GHz concluded that orbital reconstruction needed accuracies of a few centimeters (cm). This in turn required significant additional infrastructure both on board and on the ground. That is a combination of multiple spacecraft navigation techniques consisting of an onboard GPS receiver and a Satellite Laser Ranging Array (Asaki et al. 2008). While the engineering problem of sensitivity is very difficult to address, new VLBI techniques can reduce the restrictions which arise from the weight and the orbit limitations.

The rationale for S-VLBI is that it is the only method which can provide the long baselines that are required for the highest resolutions, where high frequencies are not an option. Such cases would be particularly important for astrophysical emission lines at fixed frequencies (i.e., masers), or sources for which higher frequencies are unfeasible due to their steep spectral index or changes in the structures under study.

One of the best reasons for focusing on the frequencies around 1.4 GHz is that the SKA Phase-1 site decision has recently been made, with both Western Australia and South Africa being selected to host some of the Square Kilometre

Array (SKA)-mid (i.e., frequencies around 1.4 GHz) dishes. The Australian site will host a smaller array with phased array feeds (PAFs) to perform unbiased surveys, whereas the South African site will host the majority of the antennas for high-sensitivity targeted observations. Both sites are expected to be capable of supporting phased-array VLBI observations, as this would be an extension of the pathfinder capabilities (i.e., those of ASKAP and MeerKAT). With a phased-SKA core in Australia and in South Africa, with the former capable of forming multiple beams and the latter capable of forming multiple sub-arrays, high-sensitivity VLBI baselines can be formed. High sensitivity improves astrometry, but on its own is insufficient to ensure it. With this as our driver we are investigating how to combine the Phase-1 SKA-mid with S-VLBI to achieve high-precision astrometry. Alternatively Fomalont & Reid (2004) report on approaches for achieving microarcsecond ( $\mu\text{as}$ ) astrometric accuracy with the high frequencies that will be provided by SKA-Hi. However the timeline for the installation of SKA-Hi is not yet clear.

### 1.1. L-band Astrophysics with the Longest VLBI Baselines

#### 1.1.1. Pulsar Astrometry with SKA

Pulsar astrometric VLBI is a well-established technique which measures parallaxes and proper motions, providing distances and true velocities of pulsars. It is also a key science goal for SKA, as VLBI observations of any discovered pulsar–black hole (PSR–BH) candidates will be required to determine the precise distances. This will be an essential step in the detection of gravity waves from these PSR–BH sources (Kramer et al. 2004). These sources exist in the “strong gravity” regime and would allow for the testing of predictions of quantum gravity and the search for deviations from classical general relativity (GR). The sensitivity of the SKA will lead to the discovery of many (estimated to be hundreds) of PSR–BH pairs, of which tens are expected to be millisecond pulsars. These, because of the requirements for their formation, will be close to the galactic center or in globular clusters, that is, at distances of the order of 10 kpc. The full analysis for the application of all the GR tests depends on using astrometric VLBI measurements of the trigonometric parallax to independently determine the distances to these sources. Therefore one would need to be achieving positional accuracies at the level of  $15 \mu\text{as}$  at the observing frequency of 1.6 GHz (Smits et al. 2011). This is similar to the very best astrometric accuracies currently obtained at wavelengths of one to, at most, a few cm (Reid et al. 2009 and the references therein).

#### 1.1.2. OH Masers in the Milky Way System

Hydroxyl (OH) masers as well as water vapor ( $\text{H}_2\text{O}$ ), silicon monoxide (SiO), and methanol ( $\text{CH}_3\text{OH}$ ) masers are excellent tools for astrometric studies. As for pulsars, trigonometric parallaxes have been measured for 1665 and 1667 MHz (mainline) OH masers associated with long-period variable, asymptotic giant branch (AGB) stars (van Langevelde et al. 2000; Vlemmings et al. 2003; Vlemmings & van Langevelde 2007). These are associated with massive star-forming regions, and evolved stars such as AGB and post-AGB stars. Toward the Galactic center, a large group of OH maser sources have been detected (Sjouwerman et al. 1998). Thus the OH masers are also good astrometric tracers of the dynamics of the Milky Way.

In particular, OH maser sources in the Large and Small Magellanic Clouds (LMC and SMC) are excellent targets for

S-VLBI astrometry. While Galactic OH maser spots are spatially resolved in S-VLBI (Slysh et al. 2001), those in the LMC, at a distance of  $\approx 50$  kpc, should be unresolved. There are 10 such OH maser sources known so far (Wood et al. 1986, 1992; Brooks & Whiteoak 1997; van Loon et al. 1998; Brogan et al. 2004; Roberts & Yusef-Zadeh 2005). A new OH maser survey toward the Magellanic Clouds, as part of GASKAP (Galactic ASKAP Spectral Line Survey; Dickey et al. 2013), will massively increase the number of sources. It is expected that the proper motion of each of the Magellanic masers, which are on the order of  $100 \text{ km s}^{-1}$  and correspond to a proper motion of  $\sim 400 \mu\text{as yr}^{-1}$ , will be detectable. Thanks to a larger sample size of proper motions in the galaxies ( $> 100$ ), the rotations of the LMC and the SMC may be well modeled and the orbital motion may be unambiguously determined in an accuracy significantly better than  $0.1 \text{ mas yr}^{-1}$  achieved in previous measurements (e.g., Vieira et al. 2010; Kallivayalil et al. 2013). Furthermore, the measurement of the trigonometric parallaxes of OH masers in the LMC will directly determine its distance and cement the first step in the cosmological distance ladder. To reliably detect the parallax ( $\sim 20 \mu\text{as}$ , a peak-to-peak modulation of  $\sim 40 \mu\text{as}$ ) in the individual maser spot motions will require astrometric accuracies better than this level.

#### 1.1.3. Requirements

For both science cases the aim is to achieve approximately  $15 \mu\text{as}$  astrometric accuracy. Theoretically the astrometric accuracy achievable, from statistical considerations, is approximately the synthesized beamwidth over the signal-to-noise ratio, but in practice this is typically limited to at most a hundredth of the beam (Fomalont et al. 1999). The minimum L-band beam achievable with global ground baselines is of the order of 10 milliarcseconds (mas) which, independent of any other consideration, makes the required precision a very challenging proposition, as one would be required to super-resolve the beam by three orders of magnitude. Any unstable structure at these scales or source position changes would contaminate the astrometric results, even if the methodological approach could in principle deliver that accuracy. The use of weak and barely detected sources as calibrators in PR analysis will prevent the analysis of the sources for structural changes. This is in comparison with the well-studied ICRF sources which have been monitored for structural variations over decades and at submilliarcsecond scales, which is possible as they are also monitored at higher frequencies. S-VLBI baselines will be an order of magnitude longer than global baselines, and would directly resolve and separate structures with an angular scale greater than  $\sim \text{mas}$ . This reduces the challenge, but does not remove it. Nevertheless resolving to a hundredth of the beam has been demonstrated in conventional centimeter-wavelength VLBI, so one would expect the same level to be achievable with S-VLBI and therefore provide the astrometric levels required.

There are several approaches to deliver improved astrometric accuracies at lower frequencies: GPS-based ionospheric corrections (Chatterjee 1999), wide bandwidth corrections (Briskin et al. 2003), in-beam corrections (Chatterjee et al. 2009), and multiple calibrator two-dimensional corrections (Fomalont & Kopeikin 2002; Rioja et al. 2002; Jimenez-Monferrer et al. 2010). Most astrometric campaigns have focused on the approach followed by Chatterjee et al. (2009), where the dominant residual errors in the measurements are diluted by the proximity of the calibrator to the target. The (relative) astrometric accuracy of Chatterjee’s work is  $\sim 0.1 \text{ mas}$ , which is achieved

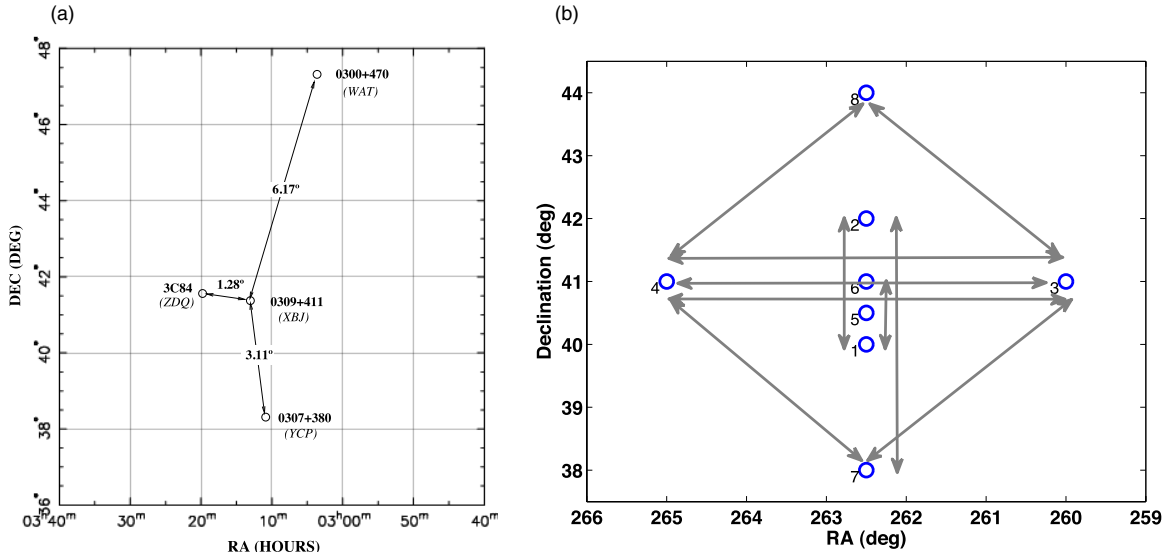


**Figure 1.** (a) Sky coverage of the four sources targeted in the original cluster–cluster demonstration (from Rioja et al. 2002). (b) Orientation of sources in these simulations, with the combinations formed indicated with light lines and triangles.

(A color version of this figure is available in the online journal.)

by using a weak source within the primary beam (typically  $\sim 10$  arcmin from the pulsar) and making the final calibration against those. Although the proper motion and parallax are measured to high precision, the ultimate astrometric accuracy is limited by the unknown (and unknowable) stability of the weak in-beam calibrator.

To achieve higher precision astrometry with a single calibrator, it must be 10 times closer to improve the astrometry 10 fold. To achieve  $10 \mu\text{as}$  one would therefore need a calibrator within an arcminute. Estimates from the simulations of likely detectable sources (Wilman et al. 2008) predict that many sources will be found in-beam, but not so many that these would have the arcmin separations required for  $\sim 15 \mu\text{as}$  level astrometry (Godfrey et al. 2012). Alternatively, to achieve the SKA goals, methods that use multiple calibrators have been proposed that interpolate solutions to the target line of sight, that is, to use the combination of *multiple* calibrators, as described by Rioja et al. (2002) and Fomalont & Kopeikin (2002), with the use of *simultaneous* in-beam calibrators, as described by Chatterjee. Such approaches to VLBI calibration are known as “cluster–cluster” or “MultiView” (Rioja et al. 1997, 2009a) VLBI.

### 1.2. MultiView VLBI

MultiView VLBI has been reviewed elsewhere (Rioja et al. 2009a), and here we only summarize the method and benefits. The MultiView approach is to use multiple high-quality calibrators arranged around the target and to reconstruct the ionospheric phase correction required in the direction of that target. The interpolation of the required phases, accounting for linear variations across the field, reduces considerably the need to have the calibrators close to the target. That is, the calibrators no longer need to be closer than 1 arcmin to provide an accuracy of  $10 \mu\text{as}$ , as for conventional PR, only that the phase screen is sufficiently linear that the interpolated solution is equivalent to this requirement. The approach is most suitable for calibration of the phase residuals from the ionosphere, which has spatial structure that is smooth over the typical separation angle of the sources.

MultiView ideally observes all the sources simultaneously so that the temporal variations do not unduly affect the results. Nevertheless, given that the ionospheric variations are slow, this approach works even with fast source switching (Fomalont & Kopeikin 2002). We are currently performing just such tests with the Australian VLBI Network, the LBA, and plan to also test the method with the Very Long Baseline Array (VLBA). We have found, in simulations, that by using MultiView approaches we can achieve an order of magnitude improvement in the astrometric accuracy compared to using single calibrators, even when the MultiView calibrators are separated by many degrees from the target. These simulations matched the preliminary investigations of Rioja et al. (1997), for which the calibrator distribution is shown in Figure 1(a). The improvement arises from the fitting of a linear surface to the calibration residuals and interpolating this model to the target position, which allows one to extend beyond the traditional ionospheric patch (which is defined only by the difference between the phase at the calibrator and that for the target). If one includes attempts to resolve phase ambiguities, one can extend the area of validity for the solutions even further. Our approach includes this by checking solutions which include up to a few additional wraps of phase and determining if the new results are better than the original.

In addition this approach removes contributions from many other major sources of calibration errors, such as the antenna clock contributions, the antenna position error, but not source structure and position errors. This calibration approach is different in character to conventional PR, where the errors are diluted by the proximity of the calibrator to the target. The limitations in this case come from the deviation of the true phase screen from the planar solution, which for a particular source separation will become more and more pronounced as lower frequencies are used. We are currently attempting MultiView calibration with long baseline LOFAR observations at 150 MHz. LOFAR is also capable of providing multiple tied array beams “pointed” at different VLBI sources, and therefore will provide an interesting exploration of the method at very low frequencies.

Previously MultiView experiments have been performed with connected arrays where different antennas, driven by a single

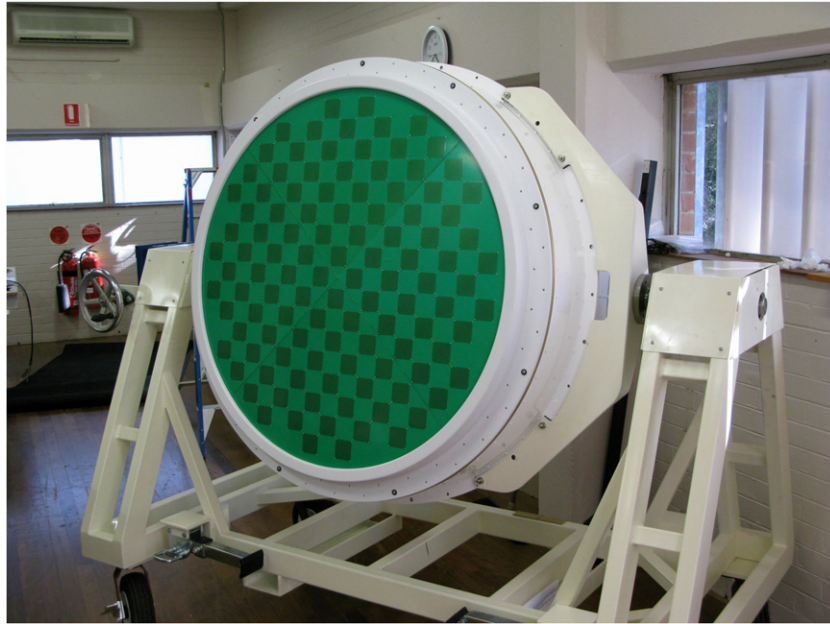


**Figure 2.** Image of the first generation “checkerboard”-type phased array feed (PAF) developed by CSIRO Australia for ASKAP (DeBoer et al. 2009). The ASKAP PAF is sensitive between 0.8 and 1.8 GHz covering a  $30 \text{ deg}^2$  field of view and is about two meters across. While this PAF has been developed for a ground-based radio array, we believe that similar technologies would be suitable for future S-VLBI instrumentation. (Image credit: R. Bolton, CSIRO).

(A color version of this figure is available in the online journal.)

time standard and under (what is approximately) a single atmosphere, are pointed simultaneously at different targets. As part of the VLBI Science Survey on ASKAP (Tingay 2009) we plan to implement MultiView methods with PAFs as installed on the ASKAP array.

### 1.3. Phase Array Feeds in Radio Astronomy

#### 1.3.1. PAF Concept and PAFs on Ground Telescopes

PAF solutions for wide-field surveys (Fisher 2010) are being developed for a number of instruments including ASKAP (DeBoer et al. 2009) and the Westerbork Synthesis Radio Telescope (WSRT; Oosterloo et al. 2010). These devices allow multiple beams to be formed on each antenna, extending the single pointing of a conventional radio dish into an instrument receiving information from multiple directions. The beams can be arbitrarily “steered” within the field of view (FoV) of the PAF, which is many times the FoV of the dish, by the electronic variation of the complex weights applied to the elements of the PAF. Figure 2 shows the PAF constructed for the ASKAP array.

These devices are most applicable for survey projects, and the wide spread interest in PAF applications arises because the large FoV optimizes the “survey speed” SVS:  $\text{SVS} \propto N_b \Omega_b B (A_{\text{eff}} / T_{\text{sys}})^2$ , where  $N_b$  is the number of beams,  $\Omega_b$  is the beamsize,  $B$  is the bandwidth,  $A_{\text{eff}}$  is the effective area, and  $T_{\text{sys}}$  is the system temperature. Assuming a fixed antenna size and system temperature the best returns come about by maximizing  $N_b B$ . However, there is also an exciting option in the VLBI field which we are actively investigating; that of applying the MultiView method in VLBI with single antennas equipped with PAFs. This forms part of the ASKAP VLBI project. In this case we are not fully covering a blank field evenly, but pointing a smaller number of tied beams at VLBI sources simultaneously, which are up to several degrees apart.

The frequency range for which PAFs will provide the best performance is 0.5–15 GHz; below 0.5 GHz aperture arrays are more efficient, above 15 GHz horn arrays can produce

many beams with conventional approaches. ASTRON, in the Netherlands, uses a “Vivaldi”-based element array in a box pattern, forming a traveling wave slot antenna between two coplanar conducting sheets (e.g., Kraus & Marhefka 2002). The approach on ASKAP is to use a connected dipole array above a ground plane in a “checkerboard” pattern on a printed circuit substrate. Each patch forms two orthogonal polarizations. The latter approach forms an extremely compact and robust structure and can be seen in Figure 2. We note that the PAF for ASKAP weighs 200 kg, but that is mainly because it is also a structural member. The weight could be much less, given that it is based around printed circuit boards.

#### 1.3.2. Phase Array Feeds in Space

We have realized that PAFs offer interesting possibilities in S-VLBI. MultiView VLBI is normally considered in terms of correcting for the approximately planar ionospheric phase-screen across each antenna. But it also corrects for any antenna position error in the same fashion. Offsets from the expected antenna positions effectively add a linear phase slope across the FoV, which is perfectly handled by the MultiView approach.

The final piece of the puzzle is the recent development of PAF technologies, which have the potential to make MultiView VLBI a straightforward and effective method. The Printed Circuit Board PAFs being developed for the ASKAP array by CSIRO are focused on meeting the wide FoV goals of the SKA, but they are equally suitable for MultiView VLBI. The new generations are falling in both cost and weight and are compact and robust.

One of the most challenging aspects of the ASTRO-G mission was to include the capability for source switching, which is essential for both detecting weak sources and astrometry, using PR. This required the inclusion of a massive Control Moment Gyro (CMG). On the other hand, the electronically steerable beams which PAFs can form would allow the tracking of multiple sources that are several degrees apart, simultaneously, without the CMG, providing much simpler antenna operations.

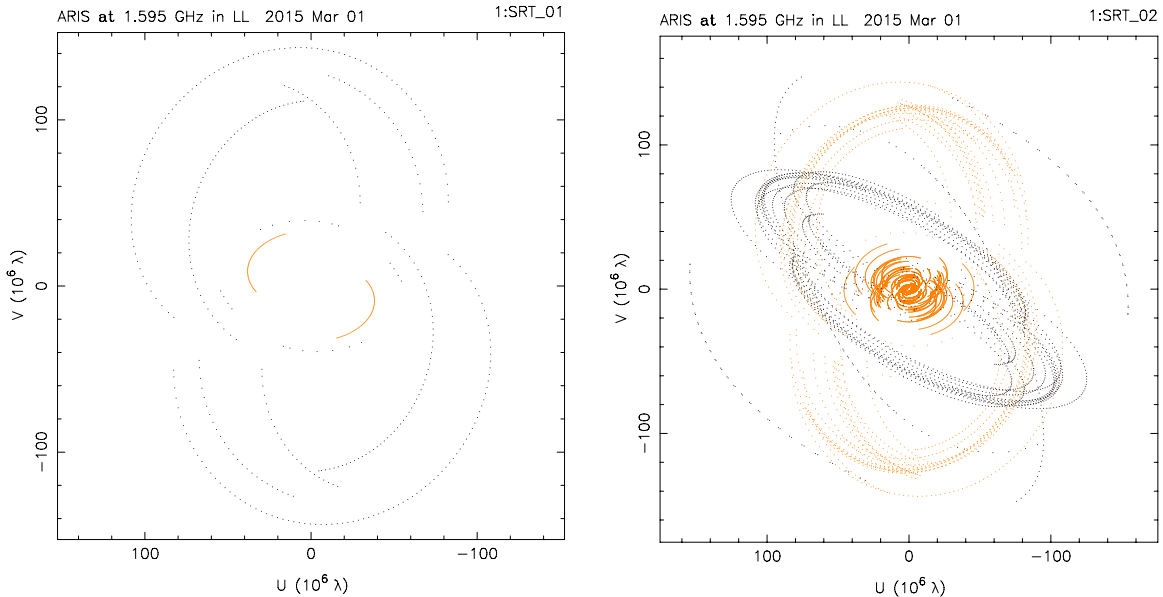


**Figure 3.** UV tracks for Source 1 in the simulations. All other sources are similar. Left: the tracks for the SKA Phase-1 model of two GRTs and one spacecraft (SRT\_01), which is highlighted. Right: the tracks for the full simulation with 10 GRTs and two spacecraft. The second spacecraft (SRT\_02) is highlighted. The ground-based baselines all fall at the center of the plot with baselines  $<40 M\lambda$ .

(A color version of this figure is available in the online journal.)

The combination of these new methods, new goals, and new technologies offers the opportunity to develop a new science mission for S-VLBI.

## 2. SIMULATIONS

We have run simulations using the software tools ARIS (Astronomical Radio Interferometer Simulator) and MeqTrees. A detailed description of ARIS can be found in Asaki et al. (2007). It is an extremely complete simulator written for the ASTRO-G mission, particularly to study the mission requirements to achieve various science goals such as PR. It allows the determination of the required observing parameters, such as the switching cycle time, the source separation angle, the Orbit Determination Discrepancy at Apogee (ODDA) accuracy of the satellite, for various tropospheric conditions, and calibrator flux densities and structures. It generates  $uv$ -data for arrays of antennas, including observational constraints (such as low elevation limits and downlink-station coverage). Among its many capabilities it will generate data sets which are contaminated by the satellite orbit error, which is the capability we have used in our simulations here. It has a simplistic ionospheric model and, as we wished to explore more sophisticated ionospheric options, we generated the ionospheric contamination with MeqTrees.

MeqTrees (Noordam & Smirnov 2010) is a python-based interface for the CASA libraries and allows the construction of many different functions into compute-trees in a straightforward and efficient fashion. We have used MeqTrees to generate the ionospheric models based on the minimum ionospheric models (MIMs) of van Bommel (2007). We have used the travelling ionospheric disturbance (TID) and the Kolmogorov models, as these are designed to reproduce the full range of observed ionospheric behavior with a limited set of parameters.

We have simulated VLBI data sets with a bandwidth of 16 MHz at 1.6 GHz with two spacecraft in ASTRO-G like orbits, plus the VLBA antennas, to provide a demonstration which would match an attractive experimental setup. Twin spacecraft missions have a number of extremely useful features,

such as the absence of any atmospheric contamination on the space-space baseline and a rapid construction of a well-sampled  $uv$  coverage on the longest baselines. The Chinese S-VLBI program is investigating a twin spacecraft mission, and this drives our configuration. However the use of twin spacecraft has little influence on the astrometric investigations discussed in this paper, as they give an improved  $uv$  coverage that provides an improved reconstruction of resolved source structure. To confirm this we have investigated the astrometric accuracy achieved for both the full simulation, which stands in for a model of a possible SKA-Phase 2 configuration, and a reduced data set which closely follows the SKA Phase 1. Figure 3 shows the typical  $uv$  coverage in both of these configurations. The sources were all modeled with 1 Jy flux and the VLBA antennas had thermal noise added based on their nominal sensitivities. In the discussions we estimate sensitivities which may be achieved in the future.

As we are particularly interested in understanding what will be possible in the near future with SKA Phase 1, we selected a smaller array to realistically model the Phase-1 response. This consists of only three stations, two on the ground and a single spacecraft. The antennas are separated by  $\sim 9000$  km as are the two Phase-1 sites of SKA-SA and SKA-AU.

The mission design of ASTRO-G continues to serve as a template for S-VLBI studies. The orbit parameters of ASTRO-G were for a periastron of 25,000 km and an orbital period of  $\sim 7.5$  hr. The mission design for PR required orbital errors of less than 10 cm. This requirement was one of the more challenging aspects for the ASTRO-G mission. In our simulations we have calibrated the data when contaminated by both an ODDA of 8 cm and 8 m, which are approximately the orbit error planned for ASTRO-G and that achieved for HALCA, respectively. These two cases are shown in Figures 4(a) and (b), respectively.

In the simulations we used the MIM TID model with two diagonal sinusoidal disturbances, a residual total electron content (TEC) level of 5 TECU ( $10^{-16}$  electrons  $m^{-2}$ ) and a 10% amplitude TID, at an altitude of 200 km with a velocity of 300 km  $hr^{-1}$ . This is shown in Figure 5(a). Our most extreme

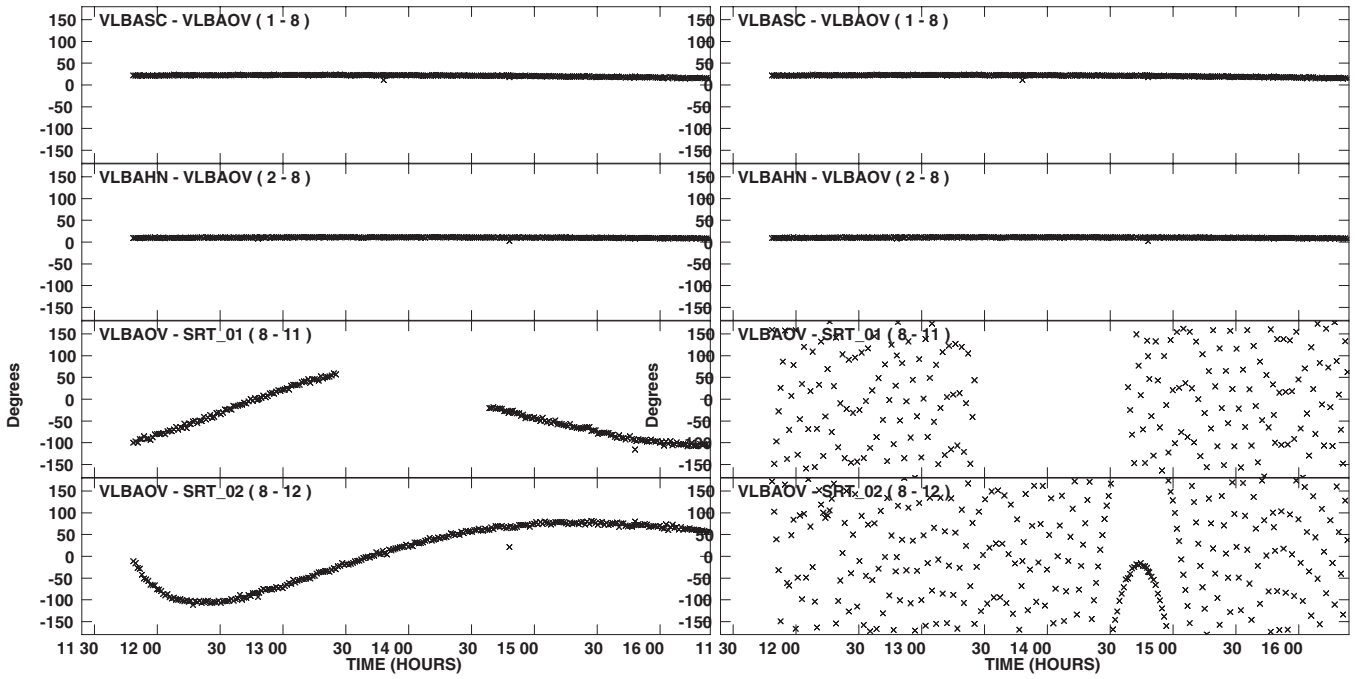


**Figure 4.** Visibility-phase plots against time, which show the effect of the positional satellite orbit errors showing two ground radio telescope (GRT) baselines (with errors of 3 mm horizontal and 10 mm vertical) and the two space-ground baselines, for an ODPA of 8 cm (left) and 8 m (right), respectively. The data are the simulation phases for a single strong source, without atmospheric contamination, that is only contaminated with position errors. The data of the GRT pair baselines show a small, approximately constant, offset from zero while those of space-ground show large variable deviations. For the 8 m case the changes are extremely rapid.

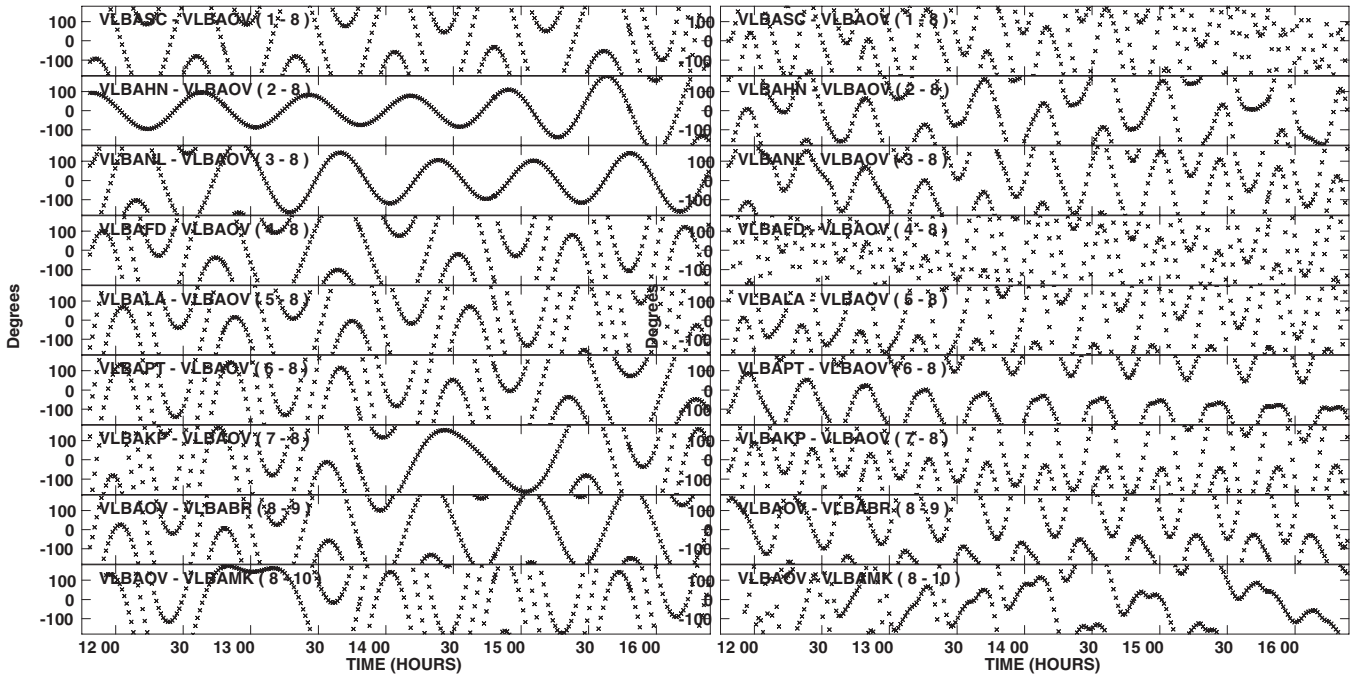


**Figure 5.** Same as Figure 3, but illustrating the effect of weather contamination only. Shown are the simulation phases in the ground baseline data for a single strong source under the weather conditions used in the simulations: the travelling ionospheric disturbance (left) and the Kolmogorov spectrum (right) with an ASD of 6 and  $12 \times 10^{-13}$ , respectively. See the text for the model details.

weather model was the MIM Kolmogorov power spectrum with  $\beta = 5/3$ , an intrinsic TEC of 10 TECU and a turbulent content of 10%, as shown in Figure 5(b). At this level, even with a self-calibration solution interval of 1 minute, the losses (13%) start to become significant. Good weather conditions are traditionally defined as having an Allan standard deviation (ASD) of  $10^{-13}$  at short timescales. Our models have ASDs of 6 and  $12 \times 10^{-13}$  at 10 s, respectively, confirming that they represent extremely bad

weather conditions for the ground stations. Other atmosphere models were explored but are not presented here, as they do not add to the discussion.

Figure 6 shows the data with large orbital errors and poor weather, calibrated with the MultiView method and the largest minimum angular separation ( $2^\circ.5$ ), overlaid with the same data calibrated in the conventional manner with the source with the smallest angular separation ( $0^\circ.5$ ). This comparison underlines

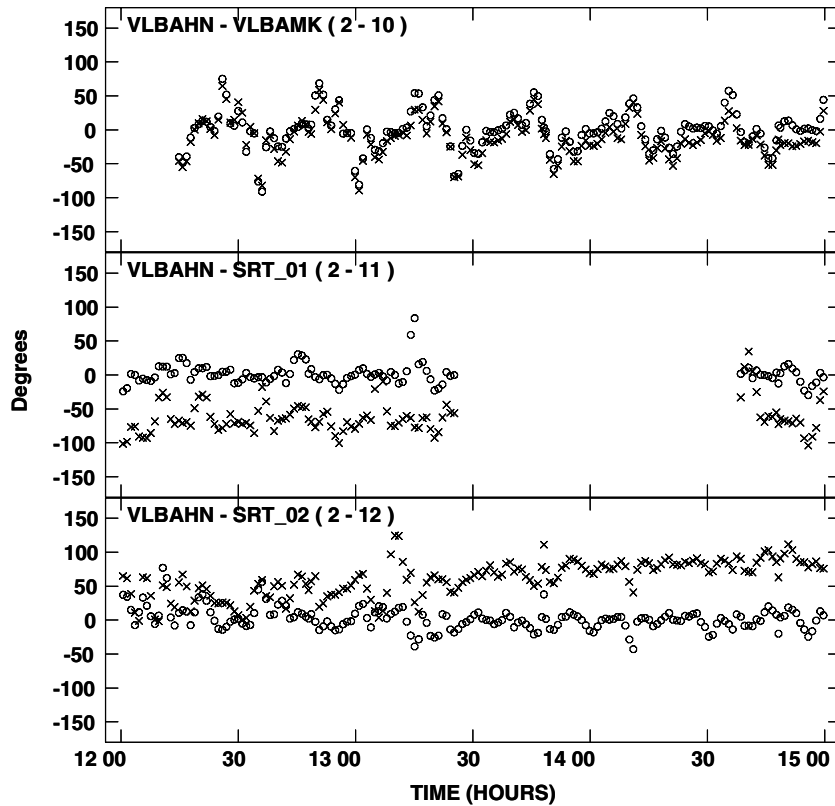


**Figure 6.** Phase residuals for the data with large orbital errors and poor weather following MultiView and conventional phase-referenced calibration. Circles mark the data calibrated following the MultiView method and the closest calibrator  $2^{\circ}.5$  from the target (Configuration 4). Overlaid with crosses are the same data conventionally calibrated with a calibrator having an angular separation of  $0^{\circ}.5$ . This underlines the improvement that the two-dimensional phase correction provides compared to the direct phase transfer.

the improvement that the two-dimensional phase correction provides compared to the direct phase transfer.

### 3. METHOD

We first simulated the  $uv$  data sets in ARIS, with only orbital errors and no atmosphere. We simulated eight sources, with the sky positions as shown in Figure 1(b). The maximum separation of the sources was  $5^{\circ}$  in right ascension and  $6^{\circ}$  in declination, which matches the ASKAP PAF FoV. Then we converted these ID-FITS data sets to measurement sets and simulated a common atmosphere for all sources with MeqTrees. The phases from the calculated models were added to those of the orbit model. Both the TID and Kolmogorov models were used, the latter with a range of parameters. Each of these measurement sets was converted back into FITS format for analysis with AIPS.

We analyzed the case of orbit only, atmosphere only, and the combination of these in our studies. Only the analyses with all effects are presented here. The residuals for each of the eight sources were measured using the AIPS task FRING and the solution tables were exported to a text file. These were read by an external script for combination with the correct weights for the source separation. We were particularly careful in the phase unwrapping (as the fractional weights were not integer values) and additionally explored the inclusion of a range of  $2\pi$  offsets around the initial results, to discover if a better solution could be identified. In this fashion we were able to significantly improve on the formation of the calibration via methods such as a linear combination of interpolations using SNCOR in AIPS.

From these sources on the sky six configurations were formed in which the “target” calibration was derived from the

weighted combinations of other calibrators. These were made up of two triangular and four linear combinations which span minimum angular separations from  $0^{\circ}.5$  to  $2^{\circ}.5$ , as listed in Table 1. Fourier inversion of these calibrated data sets, including cleaning and deconvolution, was performed with the AIPS task IMAGR.

### 4. RESULTS

We have calibrated “targets” from the combinations of calibrators as indicated in Table 1 and Figure 1(b), and Fourier inverted these data. This procedure yielded images of the target directly tied to the reference frame of the calibrators. We present MultiView-calibrated images made with the largest calibrator separations, for all models of ODDA and weather in Figure 7. In Figure 8(a), we plot the astrometric errors against the minimum calibrator distance for the SKA Phase-1 configuration. In Figure 8(b), we plot the same for the full simulation. Figures 8(c) and (d) are the same, but for the full array. We find no correlation between the minimum source separation and the astrometric errors. The mean astrometric error is  $22 \pm 10 \mu\text{s}$  for Phase 1 and  $14 \pm 8 \mu\text{s}$  for the full array. The latter achieves our original target accuracy and the former should be sufficient for the science goals. Table 2 breaks down the errors by input ODDA and weather and shows for Phase 1 that the weather quality dominates, but for the full array large orbit errors also limit the astrometry. This we interpret as being due to the random errors arising from ionosphere being diluted when there are more baselines, whereas orbital errors are not reduced because they are not independent. Similar distributions are found for the fractional recovered flux (that is the recovered flux over model

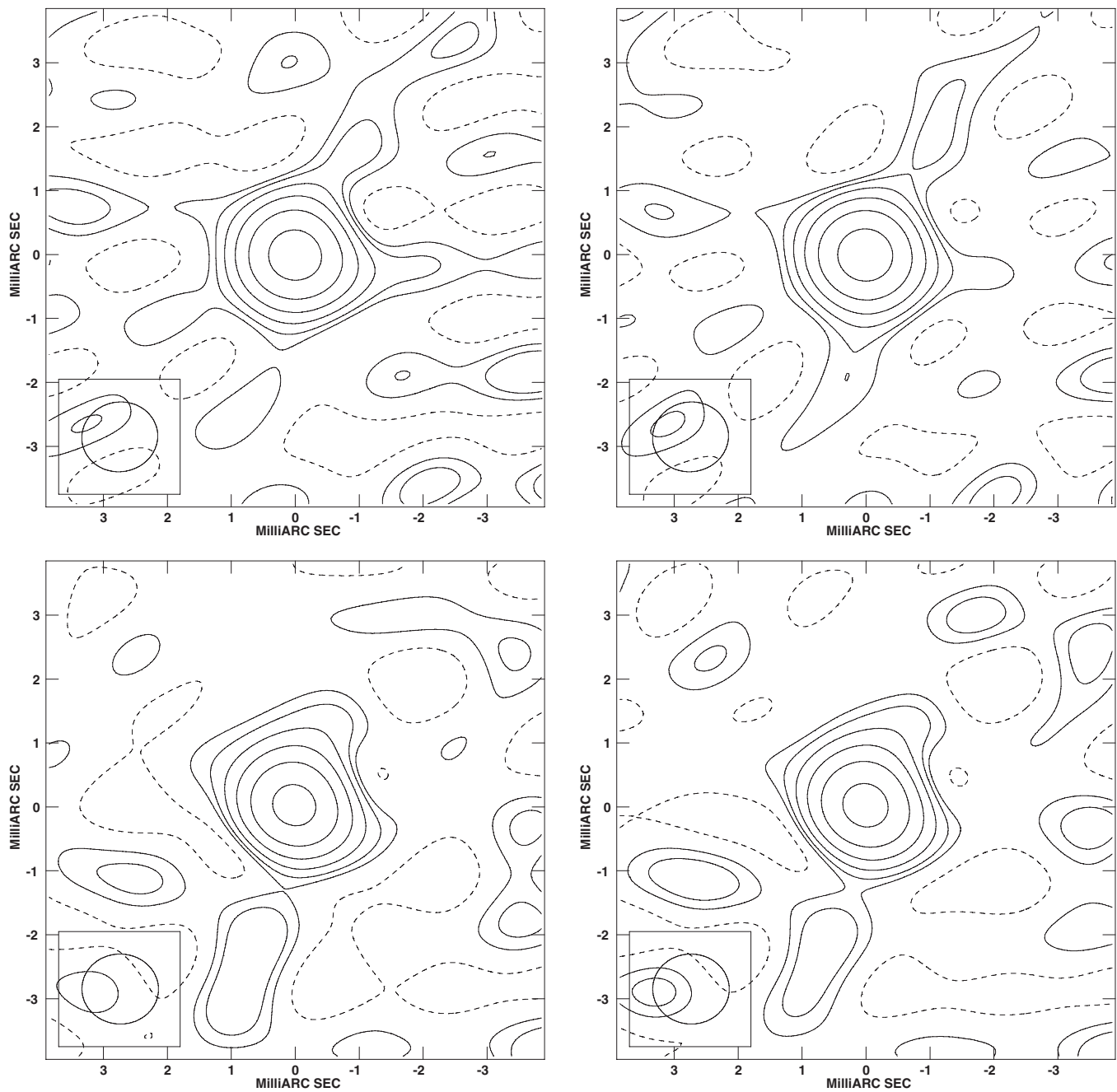


**Figure 7.** Recovered images for the Phase-1 array using Combination 4 (Source 6 calibrated with Sources 3 and 4) which has the largest source separations, contaminated with the TID (top) and the Kolmogorov models (bottom). The simulations with an ODDA of 8 cm or 8 m are on the left and right, respectively. The contours run from  $-2, 2\%$  and double thereafter. The peak flux and astrometric errors are the right most data points in Figure 8.

**Table 1**

Table of Source Combinations Used, Showing the Calibrators Involved, the Weights in the Combination, the Target Source, and the Minimum Calibrator-to-target Separation

Combination No.	Calibrator IDs			Weight (s)	Target ID	Minimum Separation (deg)	
1	1	6		1/2	...	5	0.5
2	1	2		1/2	...	6	1.0
3	2	7		3/8	...	5	1.5
4	3	4		1/2	...	6	2.5
5	3	4	8	1/2	2/3	2	2.0
6	3	4	7	1/2	5/6	5	2.5

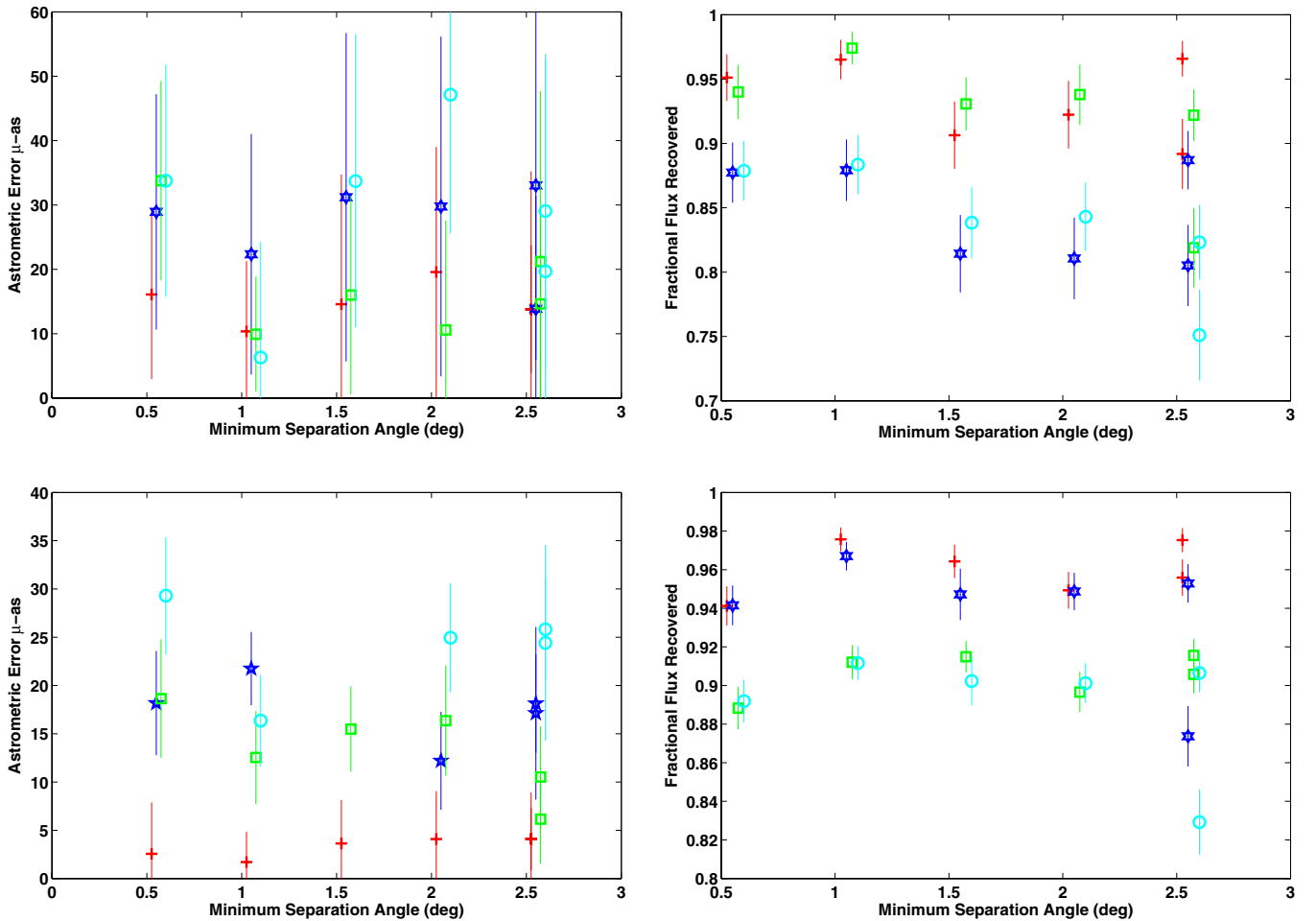


**Figure 8.** Astrometric errors and the fractional flux recovered in the recovered images as a function of the minimum calibrator distance. The upper row is for Phase-1 simulations and the lower row for the full simulation. Left: astrometric accuracy in  $\mu\text{as}$  for the four cases discussed; plus signs mark ODDA errors of 8 cm and the TID atmosphere, while squares mark the Kolmogorov atmosphere, stars mark 8 m ODDA errors and TID, while circles mark the Kolmogorov atmosphere. The error bars mark  $1\sigma$  errors from the astrometric fitting. The results have a mean error of  $22 \pm 10 \mu\text{as}$  for the SKA Phase 1 and  $14 \pm 8 \mu\text{as}$  for the full array. Right: flux recovered against minimum calibrator distance with the same symbols. The target accuracy is achieved except for the case of both very bad weather ( $\text{ASD} > 10^{-12}$ ) and relatively poor orbit errors (ODDA of 8 m). The different cases are slightly offset for clarity.

(A color version of this figure is available in the online journal.)

**Table 2**

Astrometric Errors (in  $\mu\text{as}$ ) for the Four Cases Explored: Large and Small ODDA and the Two Atmospheric Conditions, Traveling Wave Ionospheric Disturbances (TID) and Kolmogorov Spectrum (Kol)

	SKA Phase 1		Full Array	
	ODDA			
	8 cm	8 m	8 cm	8 m
TID	$15 \pm 3$	$18 \pm 9$	$3 \pm 1$	$17 \pm 3$
Kol	$27 \pm 7$	$28 \pm 14$	$13 \pm 5$	$24 \pm 5$

flux), with the flux recovered and the minimum source separation being only weakly associated. The fractional recovered flux ( $0.88 \pm 0.06$  for Phase 1 and  $0.92 \pm 0.04$  for the full array) and off-source image rms ( $6 \pm 2 \text{ mJy}$  in both cases, in line with that expected) give a dynamic range greater than a hundred. For comparison we performed conventional calibration for the closest pair (sources 6 and 5) which have an angular separation of  $0.5$ . For poor orbit reconstruction the calibration fails as shown in Figure 6, and even in the best cases it is no better than the MultiView calibration.

## 5. DISCUSSIONS

### 5.1. Achieving $15 \mu\text{as}$ Astrometry with a Simplified Spacecraft

We have demonstrated a method which allows the highest levels of astrometric accuracy to be achieved at 1.6 GHz. This involves the combinations of S-VLBI to achieve small beam sizes at the required frequency, the capability to form multiple beams simultaneously on the antennas, and MultiView analysis to solve for the two-dimensional phase surface. These approaches allow for the resolution of the sub-beam effects on the milliarcsecond-scale described in Section 1.1.3, which would contaminate and limit the astrometric accuracies, the removal of the massive CMG from the spacecraft requirements yet delivers astrometric results accurate enough to allow the measurement of parallaxes across our galaxy and out to the LMC.

The major advantages for the spacecraft from the use of MultiView methods with PAFs are: (1) the mission launch weight is reduced; (2) the source separations can be of the order of several degrees; and (3) the orbit errors can be of the order of several meters.

We have therefore shown that the MultiView method in S-VLBI can deliver the target astrometric accuracy of  $\sim 15 \mu\text{as}$

without the additional weight of a space borne CMG and the satellite navigation infrastructure. This will allow the measurement of the trigonometric parallax to PSR–BH pairs across the galaxy and OH masers in the LMC.

### 5.2. The Influence of Orbit Errors

As shown in Figure 8 the orbit errors contaminate the astrometric results, raising the mean error for an 8 cm ODDA from  $\sim 8 \mu\text{s}$  to  $\sim 20 \mu\text{s}$ , when the ODDA is 8 m. As shown in Figure 4(b) the phase rates introduced by large orbit errors become difficult to follow and at this point it would become hard to track the residuals. The HALCA orbit tracking was based on Doppler tracking at the *Ku* band, and produced orbit accuracies of the order of 5 m (Rioja et al. 2009b). A similar approach for any new mission should therefore be acceptable. Of course an iterative process could be used to estimate even larger ODDAs, from the residuals, at the correlator, which would reduce the effective ODDA to a manageable level. Such an approach could be attempted with RadioAstron.

RadioAstron was not designed for PR, let alone MultiView astrometry. Nevertheless we have considered possible approaches which could be used. With ground radio telescopes (GRTs) alternating rapidly between the four sources one would be able to remove their atmospheric contamination. RadioAstron, as it has an onboard H-maser, does not suffer from any atmospheric contamination of its own. Therefore, the cycle time between calibrators of the spacecraft could be considerably longer. Even with residual orbit errors of 8 m solution intervals of 30 minutes allow for a 65% flux recovery. Of course, the observing efficiency will be significantly reduced as the space baselines will be formed only when the GRTs were observing the same source as the space antenna.

The initial orbit errors of RadioAstron, however, are considerably greater than that of HALCA; a recent estimate is 100 m (E. Fomalont 2012, private communication). The errors arise from the influence of the moon on the very large orbit of the space craft, which prevent simple reconstruction. However one could perform a self-calibration to the spacecraft, of the best calibrator, after GRT-only calibration. The orbit errors will be smooth and should be easy to separate from the atmospheric contributions. If these errors could be corrected for one source pre-correlation and the other sources are within  $6^\circ$  (0.1 rad), the residual error will be of the order of a tenth of this absolute error. Therefore our results with ODDA residuals with 8 m should be applicable to RadioAstron.

We conclude that the orbit errors should be minimized as far as feasible, and that traditional orbit reconstruction methods should be sufficient for the MultiView method to provide high-precision astrometry. Bootstrapped calibration of larger orbit errors should be feasible, but would need to be demonstrated.

### 5.3. The Effect of the SKA Baselines

We have not directly investigated the effect of the SKA baselines on the astrometry, as that would not be significant in the setup we have used. The sources were all modeled with 1 Jy flux and the VLBA antennas had thermal noise added based on their nominal sensitivities. The SKA sensitivities are required only to detect a weak source, which we would expect to be the target. The recommended procedure is that one uses strong ICRF sources, which have been well monitored at a range of frequencies over a long time, to provide confidence in the astrometric quality of the calibrator. Both the SA and Australian

SKA arrays would be capable of supporting MultiView VLBI, either by sub-arraying or via formation of multiple outputs from their PAFs, along with conventional connected arrays such as VLBA, ATCA, GMRT, and WSRT.

With the SKA site decision now announced we can make estimates of the Phase-1 sensitivity. SKA-AU will have 96 12 m antennas with PAF receivers while SKA-SA will have 254 single pixel 13.5 m antennas. Assuming system temperatures of 30 K and 20 K, respectively, and that the SKA-SA antennas would be evenly sub-arrayed between the four sources for observation we find that these station beams have similar sensitivities of  $\sim 500 \text{ m}^2 \text{ K}^{-1}$ . For a bandwidth of 256 MHz and a 1 minute solution interval such a station correlated with a 10 m diameter antenna with a system temperature of 50 K would provide a baseline sensitivity of the order of 0.3 mJy. This underlines that S-VLBI baselines, even when combined with the SKA, will struggle to be sufficiently sensitive to detect the postulated weak in-beam calibrators; a consequence of the small diameter of any antenna capable of being launched into space. Note that this mJy limit will only be for the calibrators not the target, which would have an integration time of the whole observation. It is also worth commenting that, for VLBI with SKA Phase-1, large telescopes such as the Parkes 64 m will continue to provide significant sensitive baselines.

We conclude that S-VLBI missions can be linked to the SKA ground stations and we believe that this will be the only method that can produce the high-precision astrometry required for the fulfillment of the SKA key science goal of the measurement of trigonometric parallax distance to PSR–BH targets.

Supported in part by the CAS/SAFEA International Partnership Program for Creative Research Teams and the Strategic Priority Research Program on Space Science, the Chinese Academy of Sciences (Grant No. XDA04060700). Further support from UWA Research Collaboration Award “Studies for Technical Solutions for the Chinese S-VLBI Mission.”

## REFERENCES

- Asaki, Y., Sudou, H., Kono, Y., et al. 2007, *PASJ*, **59**, 397
- Asaki, Y., Takeuchi, H., & Yoshikawa, M. 2008, in Proc. 21st International Technical Meeting of the Satellite Division of The Institute of Navigation (ION GNSS 2008), (Manassas, VA: The Institute of Navigation), 710
- Brisken, W. F., Fruchter, A. S., Goss, W. M., Herrnstein, R. M., & Thorsett, S. E. 2003, *AJ*, **126**, 3090
- Brogan, C. L., Goss, W. M., Lazendic, J. S., & Green, A. J. 2004, *AJ*, **128**, 700
- Brooks, K. J., & Whiteoak, J. B. 1997, *MNRAS*, **291**, 395
- Chatterjee, S. 1999, Recipes for Low Frequency VLBI Phase-referencing and GPS Ionospheric Correction, Technical Report, NRAO VLBA Memo
- Chatterjee, S., Brisken, W. F., Vlemmings, W. H. T., et al. 2009, *ApJ*, **698**, 250
- DeBoer, D. R., Gough, R. G., Bunton, J. D., et al. 2009, *IEEEP*, **97**, 1507
- Dickey, J. M., McClure-Griffiths, N., Gibson, S. J., et al. 2013, *PASA*, **30**, 3
- Fisher, R. 2010, Phase Array Feeds, Technical Report, Astro2010 Tech. Dev. White Paper
- Fomalont, E., & Reid, M. 2004, *NewAR*, **48**, 1473
- Fomalont, E. B., Goss, W. M., Beasley, A. J., & Chatterjee, S. 1999, *AJ*, **117**, 3025
- Fomalont, E. B., & Kopeikin, S. 2002, in Proc. 6th EVN Symp. on New Developments in VLBI Science and Technology, ed. E. Ros, R. W. Porcas, A. P. Lobanov, & J. A. Zensus (Bonn: Max-Planck-Institut für Radioastronomie), 53
- Godfrey, L. E. H., Bignall, H., Tingay, S., et al. 2012, *PASA*, **29**, 42
- Guirado, J. C., Ros, E., Jones, D. L., et al. 2001, *A&A*, **371**, 766
- Hirabayashi, H., Hirotsawa, H., Kobayashi, H., et al. 2000, *PASJ*, **52**, 955
- Jimenez-Monferrer, S., Rioja, M. J., Dodson, R., Smirnov, O., & Guirado, J. C. 2010, in 10th European VLBI Network Symp. and EVN Users Meeting: VLBI and the New Generation of Radio Arrays (Trieste: SISSA), *PoS(10th EVN Symposium)084*

- Kallivayalil, N., van der Marel, R. P., Besla, G., Anderson, J., & Alcock, C. 2013, *ApJ*, **764**, 161
- Kardashev, N. S. 1997, *ExA*, **7**, 329
- Kramer, M., Backer, D. C., Cordes, J. M., et al. 2004, *NewAR*, **48**, 993
- Kraus, J. D., & Marhefka, R. J. 2002, *Antennas for All Applications* (New York: McGraw-Hill)
- Noordam, J. E., & Smirnov, O. M. 2010, *A&A*, **524**, A61
- Oosterloo, T., Verheijen, M., & van Cappellen, W. 2010, in Proc. 3rd Int. SKA Forum, Science Meeting (ISKAF2010): Square Kilometer Array, ed. ASTRON Netherlands Inst. Radio Astron. (Trieste: SISSA), *PoS(ISKAF2010)043*
- Reid, M. J., Menten, K. M., Zheng, X. W., et al. 2009, *ApJ*, **700**, 137
- Rioja, M., Dodson, R., Porcas, R. W., et al. 2009a, in 8th Int. e-VLBI Workshop (Trieste: SISSA), *PoS(EXPreS09)014*
- Rioja, M., Porcas, R., Dodson, R., & Asaki, Y. 2009b, in ASP Conf. Ser. 402, *Approaching Micro-Arcsecond Resolution with VSOP-2: Astrophysics and Technologies*, ed. Y. Hagiwara, E. Fomalont, M. Tsuboi, & M. Yasuhiro (San Francisco, CA: ASP), 486
- Rioja, M. J., Porcas, R. W., Desmurs, J.-F., et al. 2002, in Proc. 6th EVN Symp. on New Developments in VLBI Science and Technology, ed. E. Ros, R. W. Porcas, A. P. Lobanov, & J. A. Zensus (Bonn: Max-Planck-Institut für Radioastronomie), 57
- Rioja, M. J., Stevens, E., Gurvits, L., et al. 1997, *VA*, **41**, 213
- Roberts, D. A., & Yusef-Zadeh, F. 2005, *AJ*, **129**, 805
- Sjouwerman, L. O., van Langevelde, H. J., Winnberg, A., & Habing, H. J. 1998, *A&AS*, **128**, 35
- Slysh, V. I., Voronkov, M. A., Migenes, V., et al. 2001, *MNRAS*, **320**, 217
- Smits, R., Tingay, S. J., Wex, N., Kramer, M., & Stappers, B. 2011, *A&A*, **528**, A108
- Tingay, S. 2009, VLBI with ASKAP, Technical Report, ASKAP VLBI SSP
- van Bemmelen, I. 2007, *From Planets to Dark Energy: The Modern Radio Universe* (Trieste: SISSA), *PoS(MRU)012*
- van Langevelde, H. J., Vlemmings, W., Diamond, P. J., Baudry, A., & Beasley, A. J. 2000, *A&A*, **357**, 945
- van Loon, J. T., Zijlstra, A. A., Whitelock, P. A., et al. 1998, *A&A*, **329**, 169
- Vieira, K., Girard, T. M., van Altena, W. F., et al. 2010, *AJ*, **140**, 1934
- Vlemmings, W. H. T., & van Langevelde, H. J. 2007, *A&A*, **472**, 547
- Vlemmings, W. H. T., van Langevelde, H. J., Diamond, P. J., Habing, H. J., & Schilizzi, R. T. 2003, *A&A*, **407**, 213
- Wilman, R. J., Miller, L., Jarvis, M. J., et al. 2008, *MNRAS*, **388**, 1335
- Wood, P. R., Bessell, M. S., & Whiteoak, J. B. 1986, *ApJL*, **306**, L81
- Wood, P. R., Whiteoak, J. B., Hughes, S. M. G., et al. 1992, *ApJ*, **397**, 552